JACS
JOURNAL OF THE AMERICAN CHEMICAL SOCIETY
Article
pubs.acs.org/JACS

Visualization and Quantification of MicroRNA in a Single Cell Using Atomic Force Microscopy

Hyunseo Koo,[†] Ikbum Park,[‡] Yoonhee Lee,[†] Hyun Jin Kim,[§] Jung Hoon Jung,[§] Joo Han Lee,[§] Youngkyu Kim,*[,†] Joung-Hun Kim,*[,§] and Joon Won Park*[,†]

[†]Department of Chemistry, [‡]Division of Integrative Biosciences and Biotechnology, and [§]Department of Life Sciences, Pohang University of Science and Technology, 77 Cheongam-Ro, Nam-Gu, Pohang 37673, Korea

Supporting Information

ABSTRACT: MicroRNAs (miRNAs) play critical roles in controlling various cellular processes, and the expression levels of individual miRNAs can be considerably altered in pathological conditions such as cancer. Accurate quantification of miRNA at the single-cell level will lead to a better understanding of miRNA function. Here, we present a direct and sensitive method for miRNA detection using atomic force microscopy (AFM). A hybrid binding domain (HBD)-tethered tip enabled mature miRNAs, but not premature miRNAs, to be located individually on an adhesion force map. By scanning several sections of a micrometer-sized DNA spot, we were able to quantify the copy number of miR-134 in a single neuron and demonstrate that the expression was increased upon cell activation. Moreover, we visualized individual miR-134s on fixed neurons after membrane removal and observed 2−4 miR-134s in the area of 1.0 × 1.0 μm^2 of soma. The number increased to 8−14 in stimulated neurons, and this change matches the ensemble-averaged increase in copy number. These findings indicate that miRNAs can be reliably quantified at the single cell level with AFM and that their distribution can be mapped at nanometric lateral resolution without modification or amplification. Furthermore, the analysis of miRNAs, mRNAs, and proteins in the same sample or region by scanning sequentially with different AFM tips would let us accurately understand the post-transcriptional regulation of biological processes.

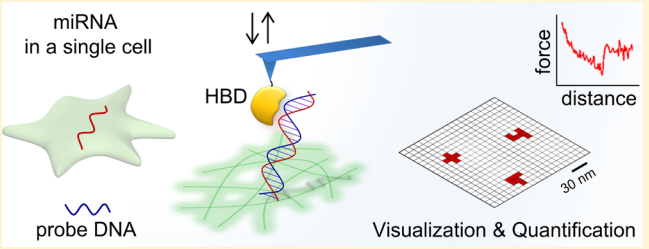

INTRODUCTION

MicroRNAs (miRNAs) are a class of short (~22 nt) noncoding single-stranded RNAs that subserve post-transcriptional modulation.[1−3] The dysregulation of miRNA expression is associated with diverse human diseases, such as cancers, cardiovascular diseases, and neurological disorders.[4−6] Indeed, analysis of miRNA levels can accurately classify tumor cells at an early stage.[7] Therefore, the quantification of miRNAs has emerged as an important topic in the biomedical field, and quantitative detection of miRNAs at the single-cell level is of great interest due to their heterogeneity among cell populations.[8−10]

Northern blotting has been regarded as the standard method for quantification of miRNAs, but it requires large amounts of total RNA for analysis and is insensitive to low-abundant miRNAs.[11,12] The similar lengths of miRNAs and standard primers have hindered direct usage of quantitative reverse-transcription PCR (qRT-PCR) to quantify miRNAs. The ligation of a universal linker, polyadenylation, or RT primers with a long overhang have been used to lengthen miRNAs, and locked nucleic acids have been inserted into primers to enhance sensitivity and selectivity.[13] However, these PCR methods have been challenged due to limited reproducibility and interplatform discrepancies.[14] In addition to PCR, various strategies for signal amplification were introduced to enhance sensitivity: (1) recycling target miRNAs, (2) labeling enzymes, (3) accumulating metal ions, and (4) coating nanoparticles with reporter oligonucleotides.[11,12,15,16] However, amplification-free detection systems can obviate the need for both multiple signal transduction steps and indirect reporter systems that are prone to error. Although nanopore sensors[17] and single-molecule fluorescence microscopes have facilitated single miRNA detection without amplification, their sensitivities are still on the order of several hundred femtomolar concentrations due to limited translocation throughput and a subpicoliter laser focal volume.[18−21]

In situ detection of intracellular miRNAs requires simple sample preparation, without cell lysis and RNA isolation, and provides additional information on the subcellular localization of miRNAs. Because Northern blotting and qRT-PCR cannot be used for *in situ* analysis, fluorophore-labeled probes including LNAs, peptide nucleic acids (PNAs), and molecular beacons have been used to measure the expression level of miRNAs in cells.[11,22,23] Carbon nanosheets including graphene derivatives, nanoparticles, and carbon nanospheres are effective carriers for intracellular delivery of probes and reversible quenchers of fluorescence signals to monitor miRNA

Received: May 16, 2016
Published: August 16, 2016

DOI: 10.1021/jacs.6b05048
J. Am. Chem. Soc. 2016, 138, 11664−11671

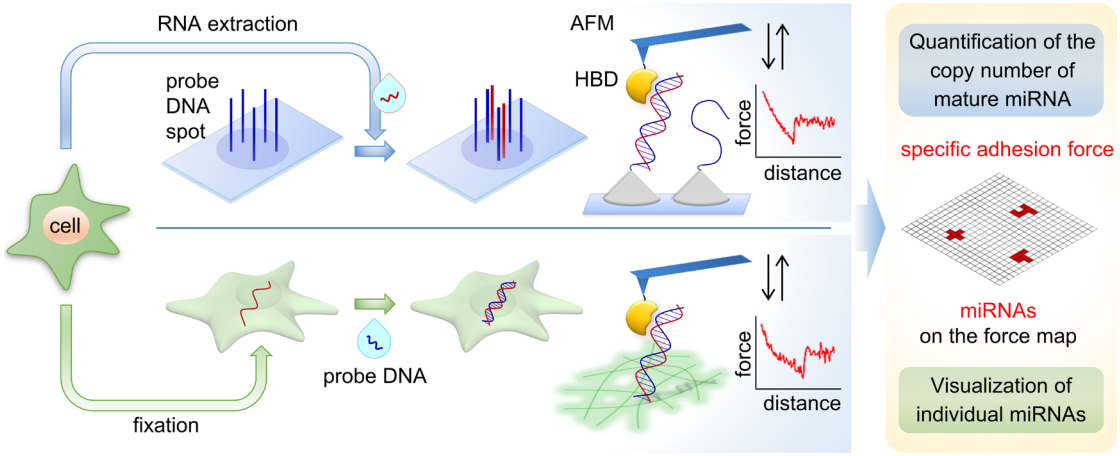

Figure 1. Detection scheme for miRNA in a single cell by tracking the single-molecular adhesion of a HBD. For the quantification of a specific miRNA, total RNA was extracted from a single cell, and target miRNAs were hybridized to a probe DNA spot. Alternatively, single cells were fixed to map the *in situ* distribution of a specific miRNA, and probe DNAs were hybridized to the immobilized miRNAs. The resultant miRNA/DNA hybrid was recognized by observing specific adhesion force−distance curves upon the approach and retraction of the HBD-tethered tip. An individual miRNA/DNA hybrid appears as a cluster of positive pixels on the adhesion force map.

expression in live cells.[22−26] Additionally to visualize the distribution of single miRNAs in a single cell, enzyme-assisted fluorescence,[8] nanoparticles,[27] and on-site rolling circle amplification[28] have been employed, but the spatial resolution of these techniques is limited due to diffraction.

Atomic force microscopy (AFM) has been used to study intra- and intermolecular interactions at the single-molecule level.[29−34] In force mapping (i.e., force volume) mode, the nanoscale distribution of target molecules can be imaged by recording force−distance (F−D) curves at a relevant interval.[35] Additionally, the absolute quantification of biomolecules by AFM force mapping has been realized by capturing molecules of interest on a well-controlled surface.[36,37] An AFM-based miRNA detection method has been reported, and an attomolar-level detection limit could be attained by monitoring the hybridization-induced change in the stiffness of probe DNA on a flat surface.[38]

Here, we demonstrate a direct approach that allows the visualization and quantification of miRNAs in a single cell without amplification or labeling of fluorescent molecules using a hybrid binding domain (HBD)-tethered AFM tip. A HBD is an N-terminal domain of human RNase H1 that binds to the RNA/DNA hybrid duplex at the minor groove in a sequence-independent manner through two independent recognition sites for RNA and DNA.[39] Whereas double-stranded RNA binding domain (dsRBD) and p19 protein that bind to dsRNA have been used to detect miRNAs with optical or electrical readout,[12,15] the use of HBD enables the employment of DNA probes rather than RNA, which is more vulnerable to degradation, and the detection of miRNAs in the intracellular space, where dsRNAs are abundant. We selectively detected mature miRNA hybridized to a complementary-DNA spot while excluding the cocaptured precursor miRNAs during the force mapping, and the discrimination of precursors was not addressed in the previous AFM-based miRNA detection method.[38]

We took advantage of this novel method to quantify miR-134, a brain-specific miRNA known to regulate spine growth and dendritogenesis.[40,41] miR-134 from a single hippocampal neuron could be quantified on a microsized spot of probe DNA. Importantly, individual miR-134s were mapped on a fixed neuron, which confirmed a significant increase in miR-134 expression upon cellular depolarization.

RESULTS

HBD-Tip Recognizes Captured miRNA. We developed a direct miRNA quantification method based on adhesion force mapping using HBD-tethered AFM tips (Figure 1). For orientation-controlled immobilization, glutathione-S-transferase (GST) was fused to the N-terminus of the HBD, and the GST−HBD was immobilized on AFM tips through a glutathione (GSH)−GST interaction. To quantify a specific miRNA in sample solution (e.g., total RNA extracted from a single cell), the amine-labeled oligonucleotide complementary to a target miRNA (i.e., probe DNA) was covalently attached to a region of a glass slide, and target miRNAs were then hybridized. Alternatively, single cells were fixed, and the plasma membrane was removed using a detergent, and then probe DNAs were hybridized to the immobilized miRNAs to map the *in situ* distribution of target miRNAs. The specific adhesion force between the HBD and the miRNA/DNA hybrid was observed at the sites where the miRNA and probe DNA hybridized to form a duplex. By recording the specific curves at a high lateral resolution, we could localize the individual miRNAs.

We used three miRNAs, miR-124, -134, and -486, to observe specific unbinding events between HBD and miRNA/DNA hybrids. Each miRNA (10 μM) was hybridized to its probe DNA spot of (1.5−2.0) × 10^2 μm in diameter (sequence information in Table S1). We performed force mapping at arbitrary positions within the corresponding spots and collected F−D curves with a nonlinear extension profile before the unbinding peak for statistical analysis (Figure S1). The most probable adhesion force values were 23, 20, and 19 pN for miR-124, -134, and -486, respectively. The adhesion force was large enough to be clearly discerned from background noise, and the values were within the known range for protein−ligand pairs.[42] Because the adhesion force between GSH and GST was measured as 92 ± 2 pN at a similar loading rate,[43] the observed force could be assigned to the unbinding between HBD and the miRNA/DNA hybrid. The average unbinding distance was 3.8 nm for the three miRNAs, a reasonable value for GST−HBD

DOI: 10.1021/jacs.6b05048
J. Am. Chem. Soc. 2016, 138, 11664−11671

stretching under the observed adhesion force. The specificity of the observed unbinding events was confirmed by examination of ssDNA, dsDNA, and dsRNA spots, and RNase H treatment (Figure S2).

The hydrodynamic radius of surface-captured molecules is a criterion to determine the optimal pixel size for quantitative analysis.[36,37] When the pixel size is sufficiently small, specific unbinding events are observed at multiple adjacent pixels according to the radius of the molecules.[44] For a pixel size of 4.0 nm, a cluster of 34 positive pixels was observed on the miR-134 (1.0 pM)-captured spot, and the probability of observing unbinding events was no less than 40% on most pixels (Figure S3). The cluster was fitted to an ellipse, and the equivalent circular radius was calculated to be 14 nm. The observed radius was in agreement with the dimension of the molecules in the bound configuration. However, no cluster was observed when the ssDNA and dsDNA spots were examined at the same resolution. Additionally, we observed clusters only when the complementary target miRNA was hybridized to the probe DNA, regardless of the presence of noncomplementary miRNA in the sample solution (Figure S4). Therefore, the individual miRNA/DNA hybrid could be mapped by observing clusters in the adhesion force map at the proper resolution, and the isolated pixels of a similar force value from a nonspecific interaction could be readily discriminated by counting only the clusters.

Selective Detection of Mature miRNAs. The production of miRNAs is tightly regulated by a series of processing steps in cells, and the abundance of a mature miRNA can differ from that of its precursor.[1,45] Accordingly, it is critical to discriminate pre-miRNAs for the accurate quantification of mature miRNAs. To investigate whether the interaction between the captured pre-miRNA and HBD showed distinct characteristics, we examined the miR-134- and pre-miR-134-captured spots (each 10 fM) sequentially.

We mapped the mature miR-134 captured spot before and after the examination of pre-miR-134 captured spot to verify the functionality of tip, and detected clusters only on the miR-134-hybridized spots but not on the pre-miR-134 spots (Figure 2 and Figure S5). When we compared the hybridization

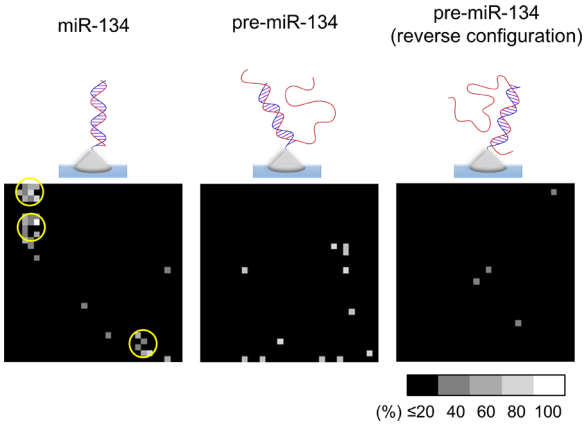

Figure 2. Selective recognition of captured miR-134. miR-134 and pre-miR-134 were hybridized separately to individual probe DNA spots. Upon examination of a spot capturing miR-134, clusters were observed in the force maps. By contrast, no cluster appeared on the spot capturing pre-miR-134. The probability of observing a specific unbinding event on each pixel is indicated in gray scale in the force maps (30 × 30 pixels, 240 × 240 nm^2).

efficiency of miR-134 and pre-miR-134 at a concentration of 10−10^4 pM using microarray, the efficiency of pre-miR-134 was 1.4−2.7 times lower than that of miR-134. Therefore, we incubated pre-miR-134 at 1000 times higher concentration (10 pM) to ensure hybridization, and interestingly, we did not observe any clusters. To assess how pre-miR-134/DNA was not recognized by the HBD-tethered tip, we examined DNA spots capturing pre-miR-134 in the reverse configuration (the probe DNA was immobilized through 3′-amine instead of 5′-amine), or pre-miR-134 missing 6-nt at the 5′ end, but were unable to detect any clusters in either case. In contrast, clusters were detected for miR-134s with an additional 3- or 6-nt overhang at the 5′ end at 10 fM (Figure S6).

These results suggest that the long RNA overhang of the pre-miR-134/DNA duplex disrupts the binding of HBD. It has been reported that the electrostatic environment determines the structural configuration of the single-stranded tail of a DNA duplex.[46,47] In a high salt concentration (100 mM Na^+), the electrostatic intrarepulsion of the single-stranded tail and inter-repulsion between the duplex and tail are minimized, and the flexible tail stays close to the duplex. Because pre-miR-134 has a 43-nt 3′ overhang upon hybridization with the probe DNA and the force mapping was performed in PBS (137 mM Na^+), the long overhang of pre-miR-134 is likely to disturb the binding of HBD to the minor groove of RNA/DNA. Thus, mature miRNAs can be selectively detected by observing clusters under a particular condition. Further studies are required to better understand the underlying mechanistic aspects.

Quantification of miR-134 in Single Cells. When we analyzed miR-134 at 10 fM (6.0 × 10^5 copies in 100 μL) on DNA spots (145−150 μm in diameter), the mean number of clusters in eight maps (240 × 240 nm^2) was 2.4 ± 0.3 (mean ± SEM). Because the number of clusters in an individual map was variable, several regions should be mapped to obtain an accurate number of target miRNAs in a sample.

Under the above parameters (spot size, force map area, and solution volume), one cluster would be observed in a map for the target miRNA concentration of 5.0 fM (3.0 × 10^5 copies). Scanning a larger region to detect miRNAs with a lower copy number is preferable; however, the scanning time would increase linearly with the sensitivity. Thus, it is necessary to reduce the size of the DNA spot to capture the target miRNAs in a smaller area, and the detection limit is enhanced by a power of square at the same scanning time. The average copy number of a given miRNA species in a cell has been estimated at approximately 500 (ref 48). To quantify a target miRNA in a single cell, a probe DNA spot of 3−8 μm diameter was produced using an AFM-based fluidic tool,[49] and the capture efficiency was evaluated by incubating a synthetic miR-134 solution of 10−100 aM (240−2400 copies in 40 μL) on one such spot (Figure 3 and Figure S7). By recording maps at three arbitrary positions within a spot for one sample and taking the average, we calculated the number of captured miR-134s on each spot. From the slope of the linear regression, we estimated the capture efficiency of miR-134 on a probe DNA spot to be 78%.

The expression level of miR-134, which regulates synaptic plasticity, increases by 2−4-fold upon depolarization of hippocampal neurons.[41] To determine the absolute copy number of miR-134 in a single cell, we extracted the total RNA from cultured mouse hippocampal neurons (DIV7) after stimulation with KCl (40 mM) for 2 h. The numbers of miR-134s in single unstimulated cells were calculated to be 285, 299,

DOI: 10.1021/jacs.6b05048
J. Am. Chem. Soc. 2016, 138, 11664−11671

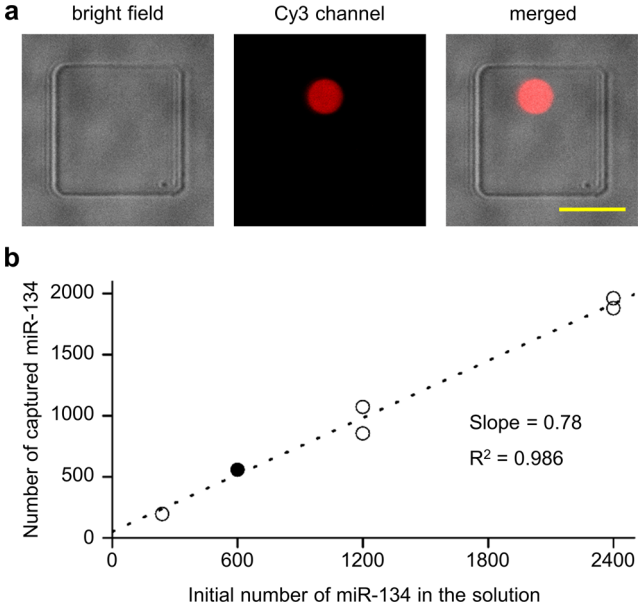

Figure 3. Capture and quantification of miR-134 on micrometer-sized spots. (a) Confocal microscope images of a probe DNA (Cy3 at the 3′ end) spot generated on a square-patterned glass slide. Scale bar, 10 μm. (b) Detection of 10−100 aM (240−2400 copies) miR-134 on separate spots (30 × 30 pixels, 300 × 300 nm^2). A filled circle indicates that two data points are overlapped. A linear correlation was observed between the number of captured miR-134 and the initial number of miR-134 in the sample solution, and the capture efficiency was calculated as 78% from the slope of linear regression.

and 374, and those in single stimulated cells were 948, 983, and 1574 (Figure 4a and Table S2). The observed average numbers

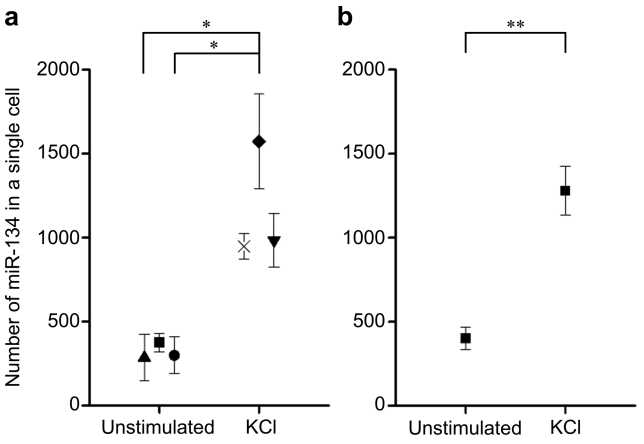

Figure 4. Quantitative analysis of miR-134 in a single neuron. Primary hippocampal neurons (DIV7) were either unstimulated or stimulated with 40 mM KCl for 2 h before RNA extraction. (a) Total RNA was extracted directly from a single neuron by micropipette aspiration. The solution was divided into two aliquots, and each aliquot was analyzed on a separate spot with an HBD-immobilized tip. Each symbol indicates the result for an individual neuron. Mean ± SEM (from two spots). Statistical comparisons between the data obtained for six cells were determined by one-way ANOVA followed by a post hoc Tukey's test. *$p < 0.05$. (b) Total RNA was extracted from neurons in a culture plate under each condition. miR-134 in the total RNA solution was quantified by qRT-PCR, and the number of miR-134 in a single neuron was calculated by assuming 20 pg of total RNA per cell.[50] $n = 3$ for each group. **$p < 0.01$ (t test).

(319 and 1168) of miR-134s in a single cell are similar to the values determined by qRT-PCR (400 ± 70 and 1300 ± 140 (mean ± SD)) (Figure 4b), and the ratios of the increase upon KCl stimulation are also comparable (3.7 from AFM vs 3.3 from qRT-PCR). Because the standard deviation observed with AFM for the unstimulated cells is 15% (data in the left part of Figure 4a) and that obtained with qRT-PCR is 16%, it can be concluded that the variation observed with AFM is comparable to that observed with conventional techniques. It is interesting to note that the AFM value for the stimulated cells is 30% (data in the right part of Figure 4a), whereas the corresponding value for qRT-PCR is 11%. Although it is premature to ascribe the larger variation to genuine cell-to-cell variation, the current analytical methodology would be sufficiently accurate to investigate such variation.

***In Situ* Mapping of miRNA in Single Cells.** To fully explore the AFM approach, we mapped the distribution of miR-134 on fixed hippocampal neurons (DIV7). After fixation, the plasma membrane was removed using a detergent, and probe DNA complementary to miR-134 was applied for the duplex formation. We observed specific $F-D$ curves on neuronal soma with the most probable adhesion force of 23 pN (Figure S8). Although the adhesion force was similar to that observed on probe DNA spots on glass slides, the unbinding distance was much longer and showed a broader distribution, whereas a single rupture event predominated. In addition, high-resolution force mapping showed clusters of positive pixels on fixed neurons (Figure S3). The shapes of the clusters varied due to differences in the local environment and random cross-linking positions of miRNAs. Nevertheless, cluster radius (10−14 nm) was comparable to that (14 nm) observed on glass substrates, and we applied the same counting criteria used for the analysis on the solid substrate to assign miRNAs on fixed cells.

We mapped the arbitrary positions of neuronal soma after hybridization with probe DNA complementary to miR-134. Neurons labeled by MAP2 immunostaining were imaged in the intermittent contact mode, and three positions were selected for adhesion force mapping (100 × 100 pixels, 1.0 × 1.0 μm^2) (Figure 5). At the soma, 2−4 clusters were observed in a map. The disappearance of clusters in the same regions after the RNase H treatment confirmed the specificity of the observed adhesion $F-D$ curves. On the fixed neurons, the qualified clusters were observed only when the probe DNA was hybridized, but not upon the hybridization of the complementary RNA or scrambled DNA (Figure S9), validating the specific detection of miRNA/DNA hybrids in agreement with the results obtained on the probe spots on glass slides. Taken together, the cluster formation in the map is most likely to be specific to the sequence of the employed DNA probe.

We analyzed the change in miR-134 expression induced by membrane depolarization on the fixed neurons. Hippocampal neurons (DIV7) were depolarized via KCl (40 mM) perfusion for 2 h before fixation. On average, 9.9 clusters were observed within the mapped areas of the stimulated neurons (1.0 × 1.0 μm^2), whereas only 2.7 clusters were detected in the unstimulated control neurons (Figure 6). The stimulation of neurons with KCl was further verified by imaging the increased expression of c-Fos with a confocal microscope (Figure S10). Although further study is required to understand the interaction depth of the AFM tip and the influence of sample preparation, the increase in cluster number observed using this direct AFM mapping was congruent with what was assessed macroscopically on probe spots with isolated RNA. The small

DOI: 10.1021/jacs.6b05048
J. Am. Chem. Soc. 2016, 138, 11664−11671

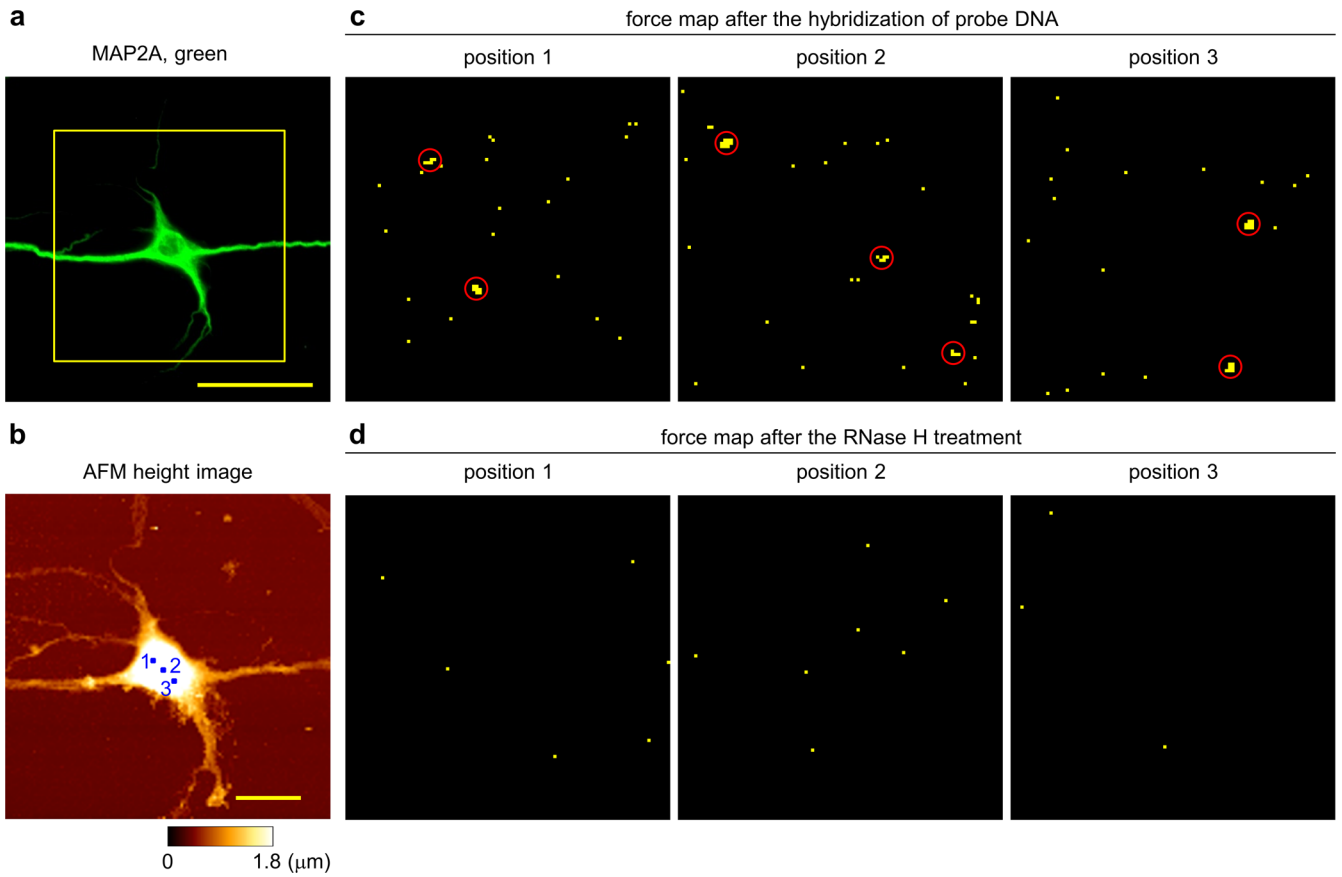

Figure 5. Mapping of miR-134 distribution on fixed neurons. (a) Primary hippocampal neurons (DIV7), MAP2; green. (b) The boxed area in panel a was imaged with AFM. (c) Numbered regions in panel b were examined by adhesion force mapping after the hybridization of miR-134 complementary DNA. (d) The same regions were re-examined after the RNase H treatment with the same tip, and no cluster was observed. (c, d) Yellow pixels indicate where specific unbinding events were observed more than once out of five measurements (100 × 100 pixels, 1.0 × 1.0 μm^2). Scale bars, 50 μm in panel a and 20 μm in panel b.

variance among the examined positions in a cell and among cells under the same condition reflects the global expression of miR-134 in the soma of hippocampal neurons at DIV7.

To determine whether this approach is applicable to other cell types, N2a cells were examined using the HBD-tips. The specific adhesion *F*−*D* curves and the most probable force and distance values for the unbinding events observed on fixed N2a cells were similar to those observed on neurons (Figure S8). Furthermore, clusters were observed only upon the hybridization of probe DNAs that were complementary to miR-134 but not upon incubation of scrambled DNA on the fixed N2a cells (Figure S11). Therefore, a given miRNA can likely be detected on various cell types without noticeable difference in the interaction between HBD and the miRNA/DNA hybrid. Collectively, the HBD-tethered AFM tip can be used to visualize individual miR-134s exposed on the exterior of fixed cells, and the copy number within the chosen map area can be reliably obtained.

DISCUSSION

Here, we established a novel miRNA quantification method based on adhesion force mapping using AFM. The sensitivity of this approach was sufficient to analyze the copy number of a specific miRNA in single cells without modification, reverse transcription, or amplification. Because the dendron-coated surface that we employed in this study has been proved to provide high SNP discrimination efficiency,[51] it would be achievable to selectively detect a target miRNA that belongs to a miRNA family of similar sequences by optimizing the capture conditions.

Importantly, *in situ* mapping of individual miRNAs seems feasible, and the measured count in a given area correlated with the miRNA change observed macroscopically. Considering the high lateral resolution of AFM, we believe this approach is applicable to other regions of neurons, such as dendrites and spines, and these sections could be examined in greater detail. Furthermore, with high-speed AFM machines,[32,33,52−54] it is expected that the whole body of a single cell can be visualized efficiently. Additionally, sectioning of fixed cells and tissues would enable the inner part of cell and specific cellular compartments to be examined.[55] We believe that this new analytical approach opens a new avenue for understanding the biological role of miRNAs and their cell-to-cell variation. In particular, the detection of small amounts of miRNA biomarkers in biological samples would enable this approach to serve as a cancer diagnostic tool.[5−7,56]

Because we can detect mRNAs and proteins using oligonucleotide- and antibody-immobilized AFM tips,[36,37] it is expected that mRNAs and proteins in the single cell can be quantified with the current approach. Furthermore, it is likely that such target molecules can be mapped on the same region by scanning with different AFM probes sequentially. Accordingly, it would let us investigate how post-transcriptional networks control biological processes at the single cell level.

DOI: 10.1021/jacs.6b05048
J. Am. Chem. Soc. 2016, 138, 11664−11671

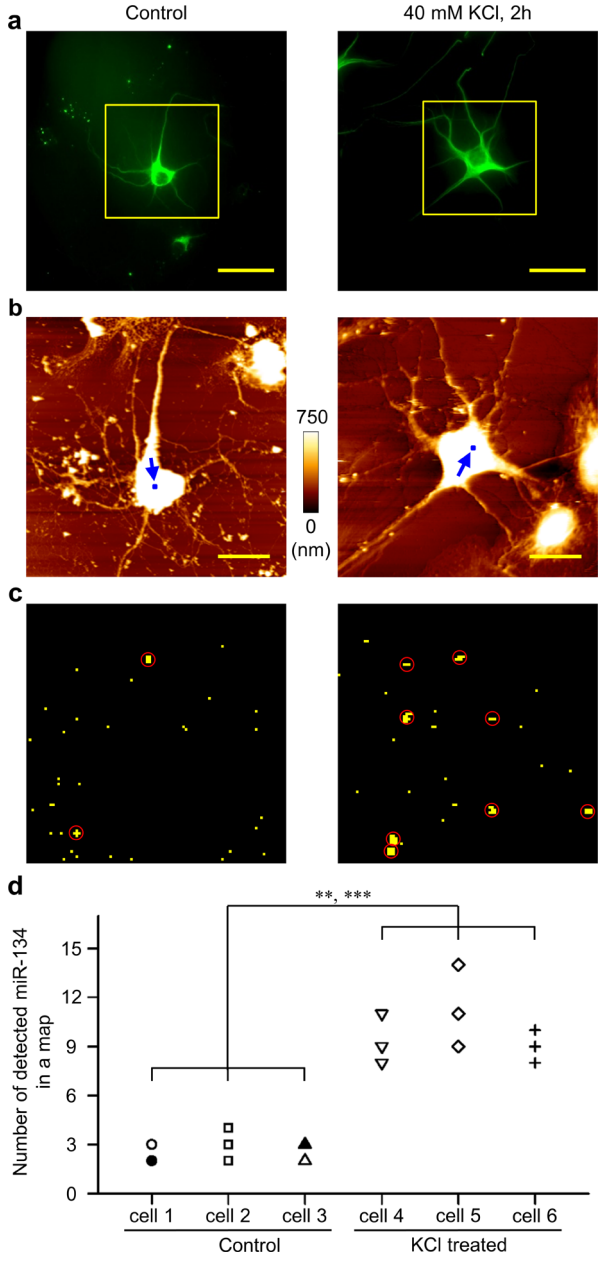

Figure 6. Visualization of the increased expression of miR-134 induced by membrane depolarization. (a) Primary hippocampal neurons (DIV7) were either unstimulated or stimulated with 40 mM KCl for 2 h before fixation and then immunostained for MAP2 (green). (b) The boxed regions in panel a were imaged with AFM. Scale bars, 50 μm in panel a and 20 μm in panel b. (c) The arbitrary positions in soma marked by a blue arrow in panel b were examined by adhesion force mapping (100 × 100, 1.0 × 1.0 μm^2). The pixels where specific adhesion force−distance curves were observed with a probability of larger than 20% are colored in yellow in the force maps. Clusters are indicated by red circles. (d) Three regions were examined for a single neuron (marked using the same legend; a filled circle or triangle indicates that two data points overlapped), and three neurons were examined under each condition. The number of detected clusters in each map is plotted. Statistical comparisons between the data obtained for six cells were determined by one-way ANOVA followed by a post hoc Tukey's test. **p < 0.01 cells 2−4, cells 2−6, and cells 3−6; ***p < 0.001 cells 1−4, cells 1−5, cells 1−6, cells 2−5, cells 3−4, and cells 3−5.

EXPERIMENTAL SECTION

AFM Tip Functionalization. AFM tips (DPN Probe Type B-1a, NanoInk and SiNi, BudgetSensors) were coated with 27-acid dendron (custom synthesis, VRND NanobioOrganics) as described previously.[37] AFM tips were oxidized in a 10% nitric acid solution at 80 °C for 20 min. The oxidized tips were silanized by reaction with *N*-(triethoxysilyl)-propyl-*O*-poly(ethylene oxide) urethane (Gelest) in a toluene solution (1.0% (v/v)) under nitrogen for 4 h with subsequent dehydration at 110 °C for 30 min. The 27-acid dendrons were immobilized on the hydroxyl surface via esterification of the dendron carboxylic groups in a dimethylformamide (DMF)/dichloromethane (DCM) (1:3, v/v) solution containing 1.0 mM 27-acid dendron, 27 mM dicyclohexylcarbodiimide, and 0.90 mM 4-dimethylaminopyridine for 12 h. Then, the protecting group at the apex of the immobilized dendrons was removed by treating with trifluoroacetic acid (1.0 M in DCM) for 2 h.

The newly generated amine group at the apex was reacted with 4-maleimidobutyric acid *N*-hydroxysuccinimide ester (GMBS) (10 mM) in an acetonitrile solution containing 10 mM *N*,*N*-diisopropylethyl amine under nitrogen for 4 h. The AFM tips were placed in stirring DMF for 20 min, rinsed with methanol, and dried under a vacuum (30−40 mTorr). Subsequently, the tips were immersed in PBS (10 mM phosphate, 2.7 mM KCl, 137 mM NaCl, pH 7.4) with glutathione (GSH) (10 mM) for 4 h, rinsed thoroughly with deionized water (Milli-Q purification system, Millipore), and dried under vacuum.

The GSH-immobilized tips were placed in PBS containing GST-fused HBD (200 nM) at room temperature for 2 h and were rinsed with PBST (0.05% Tween 20 (v/v)) and deionized water. The prepared tips were stored in PBS at 4 °C and used within a week.

Fabrication of Probe DNA Spots. All oligonucleotides were custom-synthesized at Bioneer, Inc., or Integrated DNA Technologies, Inc. (Table S1). To produce a probe DNA spot 150−200 μm in diameter, amine-labeled probe DNA (20 μM) was dissolved in 3× SSC buffer (pH 8.5) containing 0.17 mM SDS, 14.9 mM betaine, and 6.2 mM NaN_3. The DNA solution was printed onto NSB9 NHS slides (NSB POSTECH, Inc.) using a microarrayer (Q-Array Mini, Genetix) in a clean room (class 10000), and the slides were kept in a humidity chamber (85%) at room temperature for 12 h. Subsequently, the slides were placed in 2× SSPE buffer (pH 7.4) containing 7.0 mM SDS at 37 °C for 20 min with stirring and rinsed with deionized water. The residual water was removed by centrifugation at 1,000g for 1 min, and the slides were kept under vacuum (30−40 mTorr). The size of the DNA spots was measured using a fluorescence scanner (4000B scanner, Genepix).

To prepare a probe DNA spot of 3−8 μm in diameter, the probe DNA (250 μM) was dissolved in 2× SSC buffer (pH 8.5) containing 12.5% (v/v) glycerol. As a guide to locate a probe DNA spot in the AFM setup, square patterns (20 × 20 μm^2) were fabricated on NSB9 NHS glass slides via inductively coupled plasma etching before surface coating. The DNA solution was printed onto the square patterns using FluidFM (Nanosurf) with a pyramidal hollow-shaped microchannel cantilever (300 nm aperture) (Cytosurge). Incubation and washing steps were the same as described above, and the size of the spots was measured using a fluorescence microscope (Zeiss).

Hybridization of Target RNA to the Probe DNA Spot. To avoid RNase contamination, experimental tools and glassware were cleaned with RNaseZap (Ambion) and ethanol, and deionized water was treated with diethyl pyrocarbonate (DEPC, 0.05% (v/v)) for 20 h and subsequently autoclaved. An individual synthetic RNA of interest or total RNA extracted from neurons was diluted to the desired concentration in hybridization buffer (2× SSPE buffer (pH 7.4) containing 7.0 mM SDS) and denatured at 95 °C for 3 min. The denatured RNA solution (100 μL or 40 μL) was incubated on a probe DNA spot using a 4- or 8-well gasket slide and a microarray hybridization chamber (Agilent Technologies) at 34 °C for 20 h. The slide was briefly rinsed with hybridization buffer and sequentially placed in hybridization buffer and 0.2× SSC buffer at 45 °C with stirring for 15 min in each buffer. The slide was stored at 4 °C and examined within 24 h.

DOI: 10.1021/jacs.6b05048
J. Am. Chem. Soc. 2016, 138, 11664−11671

Hybridization of Probe DNA on Fixed Cells. N2a cells and neurons were fixed with 4.0% paraformaldehyde in PBS (v/v) at 4 °C for 15 min and permeabilized using 0.20% Triton X-100 in PBS (v/v) at room temperature for 10 min. The cells were washed three times in PBS at room temperature for 5 min after each step. The fixed cells were incubated in hybridization buffer containing a probe oligonucleotide (20 μM) at 34 °C for 12 h. The cells were sequentially washed in hybridization buffer, 2× SSC buffer and 0.2× SSC buffer at 60 °C with stirring for 15 min in each buffer. Then, the N2a cells were analyzed with AFM.

The fixed neurons were further processed for immunostaining. The neurons were blocked in 10% normal goat serum (in PBS (v/v), Gibco) at room temperature for 1 h and double-labeled with antibodies specific to MAP2A (MAB378 or AP20, Millipore) and c-Fos (sc-52, Santa Cruz Biotechnology) (1:500 diluted in blocking solution) at 4 °C for 1 day. Goat antibodies to mouse (Alexa 488-conjugated, AP124JA4, Millipore) and rabbit (Cy3-conjugated, 111-165-003, Jackson ImmunoResearch) (1:500 diluted in blocking solution) were used as secondary antibodies at room temperature for 90 min. The prepared samples were immediately examined by atomic force microscopy and confocal microscopy.

AFM Force Mapping and Data Analysis. For the *in vitro* quantification of miRNA, AFM force measurement was performed in freshly prepared PBS using a ForceRobot 300 (JPK Instruments) equipped with a fluorescence microscope (Zeiss). The AFM cantilever (DPN Type B-1a, NanoInk) was calibrated by the thermal fluctuation method, and the measured spring constant ranged from 3.5 to 5.5 pN nm^{-1}. The HBD-tethered AFM tip was brought over the probe DNA spot, which was marked by its fluorescence (Cy3-tagged probe DNA). Adhesion force maps were acquired by recording five force−distance (F−D) curves per pixel with an approach/retraction speed of 1.0 μm s^{-1} and z-length of 200 nm. For the approach, the maximum applied force was set as 50 pN to minimize mechanical tip damage.

To map the distribution of miRNAs, cells were examined in PBS using NanoWizard I and NanoWizard III AFMs (JPK Instruments) equipped with a fluorescence microscope (Zeiss). A silicon nitride cantilever (BudgetSensors, spring constant 20−40 pN nm^{-1}) that has tip height of 12 μm was used to examine fixed cells because the short height of the DPN tip (the value of height is not available in the specification of cantilever) caused physical interference between the cantilever and cell body. The AFM tip was located on a fixed cell, and the cell morphology was imaged in intermittent contact mode at a scan rate of 0.30 Hz (512 × 512 pixels) or in QI mode (128 × 128 pixels) before force mapping. Five F−D curves were recorded for each pixel with an approach/retraction speed of 2.0 μm s^{-1}, z-length of 800 nm, and a maximum applied force of 80−200 pN. The examined neurons were imaged using a confocal laser scanning microscope (Zeiss, LSM 510) to confirm increased c-Fos expression in the KCl-stimulated neurons.

On both probe spots and fixed cells, we acquired force maps at a pixel size of 4.0 nm to observe the hydrodynamic distance of single-molecular interaction at high resolution. To observe clusters and visualize individual miRNA/DNA hybrids in the larger area within reasonable range of time, we acquired force maps at a pixel size of 8.0−10.0 nm.

Assuming the Poisson distribution of captured miRNAs on a spot of 5 μm diameter, the 95% confidence interval for the miRNA concentration of 10 aM (240 copies in 40 μL) is 4−16 aM, and the value for 30 aM miRNA (720 copies) is 19−41 aM when three regions of 500 × 500 nm^2 are examined. The values do not overlap, but they do when three regions of 300 × 300 nm^2 are examined. Therefore, to quantify miRNAs in single cells, we examined three regions of 50 × 50 pixels (10 nm pixel size) on a probe spot to observe the difference between the control and stimulated neurons with statistical significance.

The collected F−D curves were analyzed using JPK data processing software. The baseline was corrected, and rupture force and distance were determined from the peak values. F−D curves with a linear profile (i.e., no stretching of molecules before a rupture event) were considered to be nonspecific and were excluded from further analysis. The most probable force and distance values were determined by fitting with a Gaussian curve. To measure the size of the clusters in the high-resolution force map, they were fitted to ellipses using an in-house MATLAB program.[44]

To count clusters in the force maps, the pixels of only one unbinding event per five measurements were excluded because the probability of the specific adhesion was expected to be high. Considering the hydrodynamic radius of the bound molecules and the stochastic behavior of the single-molecule interaction, the minimal number of adjacent positive pixels for a cluster was set as four or three with a pixel size of 8.0 or 10.0 nm, respectively. When the cluster size was larger than the hydrodynamic diameter (30 nm), the probability of two clusters being in proximity of one another was considered. The oversized cluster was counted as two clusters when no less than three adjacent pixels resided out of a block of 3 × 3 pixels, which corresponds to the maximum size of a cluster.

■ ASSOCIATED CONTENT

Supporting Information

The Supporting Information is available free of charge on the ACS Publications website at DOI: 10.1021/jacs.6b05048.

Additional experimental procedures, figures, and tables (Figures S1−S11, Table S1 and S2) (PDF)

■ AUTHOR INFORMATION

Corresponding Authors

*ynq.kim@gmail.com
*joungkim@postech.ac.kr
*jwpark@postech.ac.kr

Author Contributions

H. Koo and I. Park contributed equally to this work.

Notes

The authors declare the following competing financial interest(s): A patent application has been filed by POSCO and Pohang University of Science and Technology under Korean application number 10-2015-0164100: Method and apparatus for ultrasensitive quantification of microRNA.

■ ACKNOWLEDGMENTS

We appreciate kind donation of HBD constructs from Wei Yang (NIH). J.W.P. acknowledges the POSCO research fund (Project No. 2015Y040), the Brain Research Program of the National Research Foundation of Korea (Grant 2016903232), and the R&D program of MSIP/COMPA (Grant 2016K000236). J.-H.K. acknowledges grants from the National Research Foundation of Korea (Nos. 2015R1A2A1A15054037 and 2015M3C7A1027351).

■ REFERENCES

(1) Ha, M.; Kim, V. N. *Nat. Rev. Mol. Cell Biol.* **2014**, *15*, 509.
(2) Jonas, S.; Izaurralde, E. *Nat. Rev. Genet.* **2015**, *16*, 421.
(3) Bartel, D. P. *Cell* **2009**, *136*, 215.
(4) Esteller, M. *Nat. Rev. Genet.* **2011**, *12*, 861.
(5) Lujambio, A.; Lowe, S. W. *Nature* **2012**, *482*, 347.
(6) Kasinski, A. L.; Slack, F. J. *Nat. Rev. Cancer* **2011**, *11*, 849.
(7) Shell, S.; Park, S. M.; Radjabi, A. R.; Schickel, R.; Kistner, E. O.; Jewell, D. A.; Feig, C.; Lengyel, E.; Peter, M. E. *Proc. Natl. Acad. Sci. U. S. A.* **2007**, *104*, 11400.
(8) Lu, J.; Tsourkas, A. *Nucleic Acids Res.* **2009**, *37*, e100.
(9) White, A. K.; VanInsberghe, M.; Petriv, O. I.; Hamidi, M.; Sikorski, D.; Marra, M. A.; Piret, J.; Aparicio, S.; Hansen, C. L. *Proc. Natl. Acad. Sci. U. S. A.* **2011**, *108*, 13999.
(10) Porichis, F.; Hart, M. G.; Griesbeck, M.; Everett, H. L.; Hassan, M.; Baxter, A. E.; Lindqvist, M.; Miller, S. M.; Soghoian, D. Z.;

DOI: 10.1021/jacs.6b05048
J. Am. Chem. Soc. 2016, 138, 11664−11671

Kavanagh, D. G.; Reynolds, S.; Norris, B.; Mordecai, S. K.; Nguyen, Q.; Lai, C.; Kaufmann, D. E. *Nat. Commun.* **2014**, *5*, 5641.
(11) Dong, H.; Lei, J.; Ding, L.; Wen, Y.; Ju, H.; Zhang, X. *Chem. Rev.* **2013**, *113*, 6207.
(12) Hunt, E. A.; Broyles, D.; Head, T.; Deo, S. K. *Annu. Rev. Anal. Chem.* **2015**, *8*, 217.
(13) Benes, V.; Castoldi, M. *Methods* **2010**, *50*, 244.
(14) Mestdagh, P.; Hartmann, N.; Baeriswyl, L.; Andreasen, D.; Bernard, N.; Chen, C.; Cheo, D.; D'Andrade, P.; DeMayo, M.; Dennis, L.; Derveaux, S.; Feng, Y.; Fulmer-Smentek, S.; Gerstmayer, B.; Gouffon, J.; Grimley, C.; Lader, E.; Lee, K. Y.; Luo, S.; Mouritzen, P.; Narayanan, A.; Patel, S.; Peiffer, S.; Rüberg, S.; Schroth, G.; Schuster, D.; Shaffer, J. M.; Shelton, E. J.; Silveria, S.; Ulmanella, U.; Veeramachaneni, V.; Staedtler, F.; Peters, T.; Guettouche, T.; Wong, L.; Vandesompele, J. *Nat. Methods* **2014**, *11*, 809.
(15) Lautner, G.; Gyurcsányi, R. E. *Electroanalysis* **2014**, *26*, 1224.
(16) Lee, H.; Park, J. E.; Nam, J. M. *Nat. Commun.* **2014**, *5*, 3367.
(17) Johnson, R. P.; Fleming, A. M.; Beuth, L. R.; Burrows, C. J.; White, H. S. *J. Am. Chem. Soc.* **2016**, *138*, 594.
(18) Wanunu, M.; Dadosh, T.; Ray, V.; Jin, J.; McReynolds, L.; Drndić, M. *Nat. Nanotechnol.* **2010**, *5*, 807.
(19) Wang, Y.; Zheng, D.; Tan, Q.; Wang, M. X.; Gu, L. Q. *Nat. Nanotechnol.* **2011**, *6*, 668.
(20) Neely, L. A.; Patel, S.; Garver, J.; Gallo, M.; Hackett, M.; McLaughlin, S.; Nadel, M.; Harris, J.; Gullans, S.; Rooke, J. *Nat. Methods* **2006**, *3*, 41.
(21) Chan, H. M.; Chan, L. S.; Wong, R. N.; Li, H. W. *Anal. Chem.* **2010**, *82*, 6911.
(22) Dong, H.; Ding, L.; Yan, F.; Ji, H.; Ju, H. *Biomaterials* **2011**, *32*, 3875.
(23) Ryoo, S. R.; Lee, J.; Yeo, J.; Na, H. K.; Kim, Y. K.; Jang, H.; Lee, J. H.; Han, S. W.; Lee, Y.; Kim, V. N.; Min, D. H. *ACS Nano* **2013**, *7*, 5882.
(24) Dong, H.; Lei, J.; Ju, H.; Zhi, F.; Wang, H.; Guo, W.; Zhu, Z.; Yan, F. *Angew. Chem., Int. Ed.* **2012**, *51*, 4607.
(25) Choi, C. K. K.; Li, J. M.; Wei, K. C.; Xu, Y. J.; Ho, L. W. C.; Zhu, M. L.; To, K. K. W.; Choi, C. H. J.; Bian, L. M. *J. Am. Chem. Soc.* **2015**, *137*, 7337.
(26) Liao, X.; Ju, H. *Chem. Commun.* **2015**, *51*, 2141.
(27) Zhang, J.; Fu, Y.; Mei, Y. P.; Jiang, F.; Lakowicz, J. R. *Anal. Chem.* **2010**, *82*, 4464.
(28) Deng, R.; Tang, L.; Tian, Q.; Wang, Y.; Lin, L.; Li, J. *Angew. Chem., Int. Ed.* **2014**, *53*, 2389.
(29) Erdmann, M.; David, R.; Fornof, A.; Gaub, H. E. *Nat. Nanotechnol.* **2010**, *5*, 154.
(30) Li, H.; Linke, W. A.; Oberhauser, A. F.; Carrion-Vazquez, M.; Kerkvliet, J. G.; Lu, H.; Marszalek, P. E.; Fernandez, J. M. *Nature* **2002**, *418*, 998.
(31) Xue, Y.; Li, X.; Li, H.; Zhang, W. *Nat. Commun.* **2014**, *5*, 4348.
(32) Stroh, C. M.; Ebner, A.; Geretschlager, M.; Freudenthaler, G.; Kienberger, F.; Kamruzzahan, A. S.; Smith-Gill, S. J.; Gruber, H. J.; Hinterdorfer, P. *Biophys. J.* **2004**, *87*, 1981.
(33) Kim, D.; Sahin, O. *Nat. Nanotechnol.* **2015**, *10*, 264.
(34) Iyer, S.; Gaikwad, R. M.; Subba-Rao, V.; Woodworth, C. D.; Sokolov, I. *Nat. Nanotechnol.* **2009**, *4*, 389.
(35) Dufrêne, Y. F.; Martínez-Martín, D.; Medalsy, I.; Alsteens, D.; Müller, D. J. *Nat. Methods* **2013**, *10*, 847.
(36) Roy, D.; Kwon, S. H.; Kwak, J. W.; Park, J. W. *Anal. Chem.* **2010**, *82*, 5189.
(37) Jung, Y. J.; Albrecht, J. A.; Kwak, J. W.; Park, J. W. *Nucleic Acids Res.* **2012**, *40*, 11728.
(38) Husale, S.; Persson, H. H.; Sahin, O. *Nature* **2009**, *462*, 1075.
(39) Nowotny, M.; Cerritelli, S. M.; Ghirlando, R.; Gaidamakov, S. A.; Crouch, R. J.; Yang, W. *EMBO J.* **2008**, *27*, 1172.
(40) Schratt, G. M.; Tuebing, F.; Nigh, E. A.; Kane, C. G.; Sabatini, M. E.; Kiebler, M.; Greenberg, M. E. *Nature* **2006**, *439*, 283.
(41) Fiore, R.; Khudayberdiev, S.; Christensen, M.; Siegel, G.; Flavell, S. W.; Kim, T. K.; Greenberg, M. E.; Schratt, G. *EMBO J.* **2009**, *28*, 697.
(42) Lee, C. K.; Wang, Y. M.; Huang, L. S.; Lin, S. *Micron* **2007**, *38*, 446.
(43) Kim, I. H.; Lee, H. Y.; Lee, H. D.; Jung, Y. J.; Tendler, S. J.; Williams, P. M.; Allen, S.; Ryu, S. H.; Park, J. W. *Anal. Chem.* **2009**, *81*, 3276.
(44) Lee, Y.; Kwon, S. H.; Kim, Y.; Lee, J. B.; Park, J. W. *Anal. Chem.* **2013**, *85*, 4045.
(45) Schmittgen, T. D.; Lee, E. J.; Jiang, J.; Sarkar, A.; Yang, L.; Elton, T. S.; Chen, C. *Methods* **2008**, *44*, 31.
(46) Lee, I. B.; Hong, S. C.; Lee, N. K.; Johner, A. *Biophys. J.* **2012**, *103*, 2492.
(47) Lee, N. K.; Johner, A.; Lee, I. B.; Hong, S. C. *Eur. Phys. J. E: Soft Matter Biol. Phys.* **2013**, *36*, 57.
(48) Liang, Y.; Ridzon, D.; Wong, L.; Chen, C. *BMC Genomics* **2007**, *8*, 166.
(49) Grüter, R. R.; Vörös, J.; Zambelli, T. *Nanoscale* **2013**, *5*, 1097.
(50) Schmid, A.; Kortmann, H.; Dittrich, P. S.; Blank, L. M. *Curr. Opin. Biotechnol.* **2010**, *21*, 12.
(51) Hong, B. J.; Oh, S. J.; Youn, T. O.; Kwon, S. H.; Park, J. W. *Langmuir* **2005**, *21*, 4257.
(52) Ando, T.; Kodera, N.; Takai, E.; Maruyama, D.; Saito, K.; Toda, A. *Proc. Natl. Acad. Sci. U. S. A.* **2001**, *98*, 12468.
(53) Rico, F.; Gonzalez, L.; Casuso, I.; Puig-Vidal, M.; Scheuring, S. *Science* **2013**, *342*, 741.
(54) Brown, B. P.; Picco, L.; Miles, M. J.; Faul, C. F. *Small* **2013**, *9*, 3201.
(55) Kim, J. S.; Park, Y. S.; Nam, H. G.; Park, J. W. *RSC Adv.* **2015**, *5*, 18858.
(56) Rosenfeld, N.; Aharonov, R.; Meiri, E.; Rosenwald, S.; Spector, Y.; Zepeniuk, M.; Benjamin, H.; Shabes, N.; Tabak, S.; Levy, A.; Lebanony, D.; Goren, Y.; Silberschein, E.; Targan, N.; Ben-Ari, A.; Gilad, S.; Sion-Vardy, N.; Tobar, A.; Feinmesser, M.; Kharenko, O.; Nativ, O.; Nass, D.; Perelman, M.; Yosepovich, A.; Shalmon, B.; Polak-Charcon, S.; Fridman, E.; Avniel, A.; Bentwich, I.; Bentwich, Z.; Cohen, D.; Chajut, A.; Barshack, I. *Nat. Biotechnol.* **2008**, *26*, 462.

DOI: 10.1021/jacs.6b05048
J. Am. Chem. Soc. 2016, 138, 11664−11671